



# Artificial intelligence-based full aortic CT angiography imaging with ultra-low-dose contrast medium: a preliminary study

Zhen Zhou<sup>1</sup> · Yifeng Gao<sup>1</sup> · Weiwei Zhang<sup>2</sup> · Kairui Bo<sup>1</sup> · Nan Zhang<sup>1</sup> · Hui Wang<sup>1</sup> · Rui Wang<sup>1</sup> · Zhiqiang Du<sup>1</sup> · David Firmin<sup>3,4</sup> · Guang Yang<sup>3,4</sup> · Heye Zhang<sup>2</sup> · Lei Xu<sup>1</sup>

Received: 9 February 2022 / Revised: 16 May 2022 / Accepted: 20 June 2022 / Published online: 5 July 2022  
© The Author(s), under exclusive licence to European Society of Radiology 2022, corrected publication 2022

## Abstract

**Objectives** To further reduce the contrast medium (CM) dose of full aortic CT angiography (ACTA) imaging using the augmented cycle-consistent adversarial framework (Au-CycleGAN) algorithm.

**Methods** We prospectively enrolled 150 consecutive patients with suspected aortic disease. All received ACTA scans of ultra-low-dose CM (ULDCM) protocol and low-dose CM (LDCM) protocol. These data were randomly assigned to the training datasets ( $n = 100$ ) and the validation datasets ( $n = 50$ ). The ULDCM images were reconstructed by the Au-CycleGAN algorithm. Then, the AI-based ULDCM images were compared with LDCM images in terms of image quality and diagnostic accuracy.

**Results** The mean image quality score of each location in the AI-based ULDCM group was higher than that in the ULDCM group but a little lower than that in the LDCM group (all  $p < 0.05$ ). All AI-based ULDCM images met the diagnostic requirements (score  $\geq 3$ ). Except for the image noise, the AI-based ULDCM images had higher attenuation value than the ULDCM and LDCM images as well as higher SNR and CNR in all locations of the aorta analyzed (all  $p < 0.05$ ). Similar results were also seen in obese patients ( $BMI > 25$ , all  $p < 0.05$ ). Using the findings of LDCM images as the reference, the AI-based ULDCM images showed good diagnostic parameters and no significant differences in any of the analyzed aortic disease diagnoses (all  $K$ -values  $> 0.80$ ,  $p < 0.05$ ).

**Conclusions** The required dose of CM for full ACTA imaging can be reduced to one-third of the CM dose of the LDCM protocol while maintaining image quality and diagnostic accuracy using the Au-CycleGAN algorithm.

## Key Points

- The required dose of contrast medium (CM) for full ACTA imaging can be reduced to one-third of the CM dose of the low-dose contrast medium (LDCM) protocol using the Au-CycleGAN algorithm.
- Except for the image noise, the AI-based ultra-low-dose contrast medium (ULDCM) images had better quantitative image quality parameters than the ULDCM and LDCM images.
- No significant diagnostic differences were noted between the AI-based ULDCM and LDCM images regarding all the analyzed aortic disease diagnoses.

**Keywords** Aortic CT angiography · Augmented cycle-consistent adversarial framework · Contrast medium · Image quality · Diagnostic accuracy

---

Zhen Zhou and Yifeng Gao contributed equally to this work and share first authorship.

Lei Xu  
leixu2001@hotmail.com

<sup>1</sup> Department of Radiology, Beijing Anzhen Hospital, Capital Medical University, No. 2, Anzhen Road, Chaoyang District, Beijing 100029, China

<sup>2</sup> School of Biomedical Engineering, Sun Yat-Sen University, Guangzhou, China

<sup>3</sup> Cardiovascular Research Centre, Royal Brompton Hospital, London SW3 6NP, UK

<sup>4</sup> National Heart and Lung Institute, Imperial College London, London SW7 2AZ, UK

## Abbreviations

ACTA	Aortic CT angiography
AI	Artificial intelligence
ASiR-V	Adaptive statistical iterative reconstruction-V
Au-CycleGAN	Augmented cycle-consistent adversarial framework
BMI	Body mass index
CNR	Contrast-to-noise ratio
DLIR	Deep learning image reconstruction
LDCM	Low-dose contrast medium
SNR	Signal-to-noise ratio
ULDCM	Ultra-low-dose contrast medium

## Introduction

Aortic diseases may have an acute symptom, and rapid diagnosis and decision-making are needed to reduce the extremely poor prognosis. Aortic computed tomography angiography (ACTA), with high accuracy and reproducibility in the assessments of aortic morphology, plays a central role in the diagnosis, risk stratification, and management of aortic diseases [1]. However, the administration of iodinated contrast medium (CM), which may cause CM-induced acute kidney injury (CI-AKI), or renal failure, is one of the most important drawbacks of CTA [2]. Therefore, it is necessary to find an approach that enables a substantial reduction of the CM dose in CTA examinations.

Low tube voltage and energy spectrum CT technology are the most commonly used approaches to reduce the CM dose in clinical practice [3, 4]. However, reducing the tube voltage drastically may affect the diagnostic accuracy by increasing the image noise and beam-hardening artifacts. Although using the iterative reconstruction (IR) technique [5], the CTA scan with low tube voltage is not still suitable for patients with high BMI and it has not solved the problem of iodine load effectively. Energy spectrum CT also holds great promise for CM dose reduction, but it is time-consuming and its cross-scattered radiation can produce artifacts and affect the diagnostic confidence [6, 7]. Therefore, new technologies that further reduce the iodine load without compromising the image quality are needed.

Artificial intelligence (AI) is of interest owing to its potential in reconstructing CT images [8]. AI algorithm has been applied in lesion classification [9], structure segmentation [10], lesion detection [11, 12], and risk prediction [13, 14]. Recently, denoising and improving the image quality of the low-tube-voltage CT images by using AI algorithms has been investigated, which indicates a potential for further CM dose reduction [15–17].

However, there are limited AI studies aiming to improve the visual enhancement degree of CTA images with ultra-low-dose CM (ULDCM) in order to further reduce the CM dose

and minimize the iodine load of patients receiving CTA scans. In this study, we attempted to improve the enhancement appearance of ULDCM ACTA images by using a new augmented cycle-consistent adversarial framework (Au-CycleGAN) algorithm. This preliminary study aimed to evaluate the feasibility of the Au-CycleGAN algorithm in further reducing the CM dose of full aortic CT angiography (ACTA) imaging.

## Materials and methods

### Study protocol

We prospectively enrolled 150 consecutive patients between April 2019 and December 2021. All patients were referred for clinically indicated ACTA owing to known or suspected aortic artery disease. Patients with renal insufficiency (estimated glomerular filtration rate  $< 60 \text{ ml min}^{-1} 1.73 \text{ m}^{-2}$ ), allergy to CM, or the inability to perform breath-holding were excluded (Fig. 1). The study was approved by the local ethics committee, and all patients provided written informed consent.

### Scanning protocols

To limit the total dose of CM and radiation, we selected a low tube voltage, CM dose, and iodine delivery rate adapted to the BMI. The tube voltage was set to 80 kV, and 40–50 ml CM was administrated with an iodine delivery rate of 1.6 g I/ml in the scan of patients with a BMI  $\leq 25 \text{ kg/m}^2$ . When  $25 \text{ kg/m}^2 < \text{BMI} < 30 \text{ kg/m}^2$  (or  $\text{BMI} < 30 \text{ kg/m}^2$ ), the tube voltage was set to 100 kV (or 120 kV) and 50–60 ml (or 60–70 ml) CM was administrated with an iodine delivery rate of 1.8 g I/ml (or 2.0 g I/ml) (Fig. 1). All patients received an ULDCM ACTA scan with 40–70 ml mixed CM (iodixanol 320 (320 mg I/ml): saline = 1:2) using a 256-row multi-detector CT scanner (Revolution CT, GE Healthcare). After 1 h, a LDCM ACTA scan started with the same dose of pure CM (iodixanol 320, 320 mg I/ml, GE Healthcare) and the same delivery rate as the ULDCM protocol, when the CM administrated in the ULDCM ACTA scan was washed out. The coverage area and scan parameters were identical in the ULDCM protocol and LDCM protocol (thickness, 0.625 mm; interval, 0.625 mm; collimation, 256  $\times$  0.625 mm; pitch, 0.992; rotation time, 0.28 s; matrix, 512  $\times$  512). Automatic tube current modulation technique was also used. A region of interest (ROI) was placed in the ascending aorta, and image acquisition was triggered after the signal density reached a visually detectable threshold (120 HU) (bolus tracking). All raw data of the two protocols were reconstructed using an IR algorithm (ASiR-V™; GE Healthcare) (strength level, 70%).

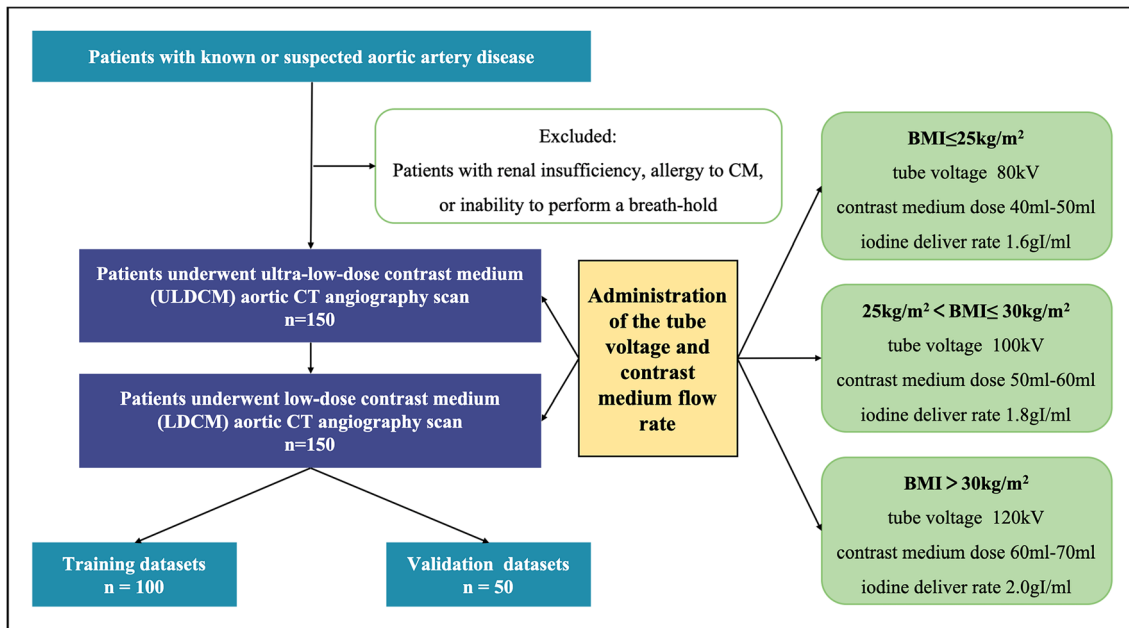


**Fig. 1** Flowchart of the study population enrollment and the administration of the tube voltage and contrast medium flow rate

Machine-generated CT dose index volume ( $\text{CTDI}_{\text{vol}}$ ) and dose-length product (DLP) values were recorded for each patient. Size-specific dose estimates (SSDE) were calculated by multiplying the  $\text{CTDI}_{\text{vol}}$  with a specific f-s coefficient based on the effective diameter [18]. Effective dose (ED) was calculated by multiplying the DLP with a conversion factor,  $k = 0.014 \text{ mSvGy}^{-1} \text{ cm}^{-1}$  [19].

### Applying the AI-based visual enhancement algorithm to the ACTA images

The ULDCM ACTA images were reconstructed with an Au-CycleGAN algorithm that leverages the cycle-consistent adversarial model to establish the mapping relationship between the unpaired ULDCM ACTA images and the LDCM ACTA images [20–22]. The ULDCM and LDCM images are not in one-to-one correspondence because of the organ motion and breathing of the patients. Hence, our Au-CycleGAN aims to establish the mapping relationship between the CTA sequences instead of the images.

The framework consists of two sub-modules:  $(G, R, D_Y)$  and  $(R, G, D_X)$ , as shown in Fig. 2.  $G$  and  $R$  denote the generators, and  $D_Y$  and  $D_X$  denote the discriminators. The two sub-modules have similar data transformation process and training manner. Taking  $(G, R, D_Y)$  as an example,  $G$  generates the CTA images with a visually enhanced aorta, and  $D_Y$  distinguishes between the generated images with visually enhanced aorta and LDCM ACTA images [23].  $R$  reversely reconstructs the ULDCM ACTA images from the generated images with the visually enhanced aorta and to make the generated ULDCM ACTA images consistent with the input

ULDCM ACTA images. In the generators, Au-CycleGAN integrates the encoder-decoder architecture and residual learning mechanism to learn multiscale features [24, 25]. The discriminator  $D_Y$  adopts the architecture of continuous convolutions with instance normalization and LeakyReLU activations [26].

The input and output of generative networks are both of size  $512 \times 512$  CTA images. The inputs of discriminator networks are the generative and LDCM images, and its output are two  $32 \times 32$  feature maps. Once the Au-CycleGAN is trained, only  $G$  is used to enhance the aorta in ULDCM CTA images. The final error formula is as follows:

$$\begin{aligned} \mathcal{L}_{\text{total}} = & \mathcal{L}_{\text{adv}}(G, D_Y, X, Y) + \mathcal{L}_{\text{adv}}(R, D_X, Y, X) \\ & + \lambda \mathcal{L}_{\text{cycle}}(G, R) \end{aligned}$$

where  $\mathcal{L}_{\text{adv}}(G, D_Y, X, Y)$  and  $\mathcal{L}_{\text{adv}}(R, D_X, Y, X)$  denote adversarial losses, and  $\mathcal{L}_{\text{cycle}}(G, R)$  denotes cycle consistency loss.  $\lambda$  is the weight coefficient that controls their relative importance, which is set to 10.

The overview of Au-CycleGAN is given in Fig. 2, and the details are provided in the [Supplementary material](#).

### Qualitative image analysis

All images (including AI-based ULDCM images, ULDCM images, and LDCM images) were processed on a dedicated workstation (Vitrea FX3.0, Toshiba) to produce maximum-intensity projections and volume-rendering images (Figs. 3 and 4). Two board-certified radiologists (N.Z. and H.W., with 5 and 7 years of

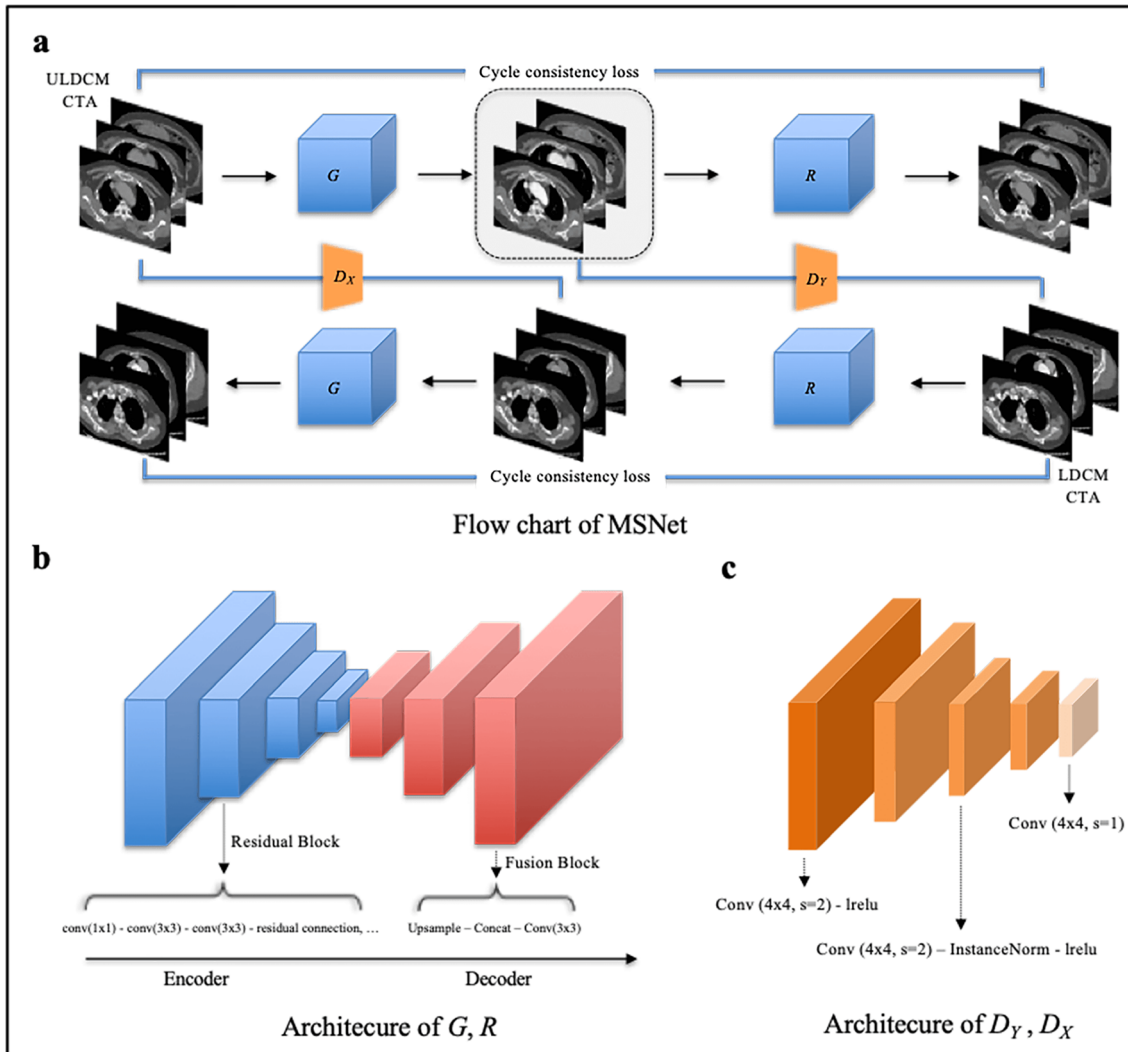


**Fig. 2** Overview of the Au-CycleGAN algorithm. **a** The flowchart of MSNet. The ultra-low-dose contrast medium CT angiography (ULDCM CTA) images and low-dose contrast medium (LDCM) CTA images were used as the input for the Au-CycleGAN. The generator  $G$  was used to generate CTA images similar to LDCM CTA (ULDCM CTA) images. The discriminator  $D_Y$  ( $D_X$ ) attempted to decipher whether the generated CTA and LDCM CTA (ULDCM CTA) images had the same intensity distribution.  $R$  recovered the generated CTA

images toward the ULDCM CTA (LDCM CTA) images. Two-cycle consistency losses were applied to calculate the similarity between the recovered images and the input ULDCM CTA (LDCM CTA) images. In the validation and testing processes, the ULDCM CTA images were input into the trained  $G$ , and the output of  $G$  were the desired CTAs (as shown in the dotted frame). **b** The detailed architectures of generators  $G$  and  $R$ . **c** The detailed architectures of discriminators  $D_Y$  and  $D_X$

experience in ACTA imaging, respectively), who were blinded to the scan conditions and reconstruction settings, independently evaluated the image quality using a 5-point scale: 5 = excellent contrast with rare overall image noise or artifact and very clear vessel margin; 4 = good contrast with slightly overall image noise or artifact and distinct vessel margin; 3 = satisfactory contrast with moderate overall image noise or artifact and identifiable, partially blurred vessel margin; 2 = detectable contrast with high overall image noise or artifact and blurred, not clear vessel margin; 1 = poor contrast with severe and unacceptable overall image noise or artifact and vessel margin

cannot be defined (visual examples shown in Supplementary material Figure S1). The consensus agreement should be reached. If not, a third senior cardiovascular radiologist with > 15 years' experience was invited to adjudicate the differences and get a final score.

### Quantitative image analysis

The two experienced radiologists also performed objective assessments on axial images and recorded the following findings: (1) mean CT attenuation value ( $CT_{Ao}$ ) and standard deviation (SD) value ( $SD_{Ao}$ ) of the ascending aorta (2 cm above

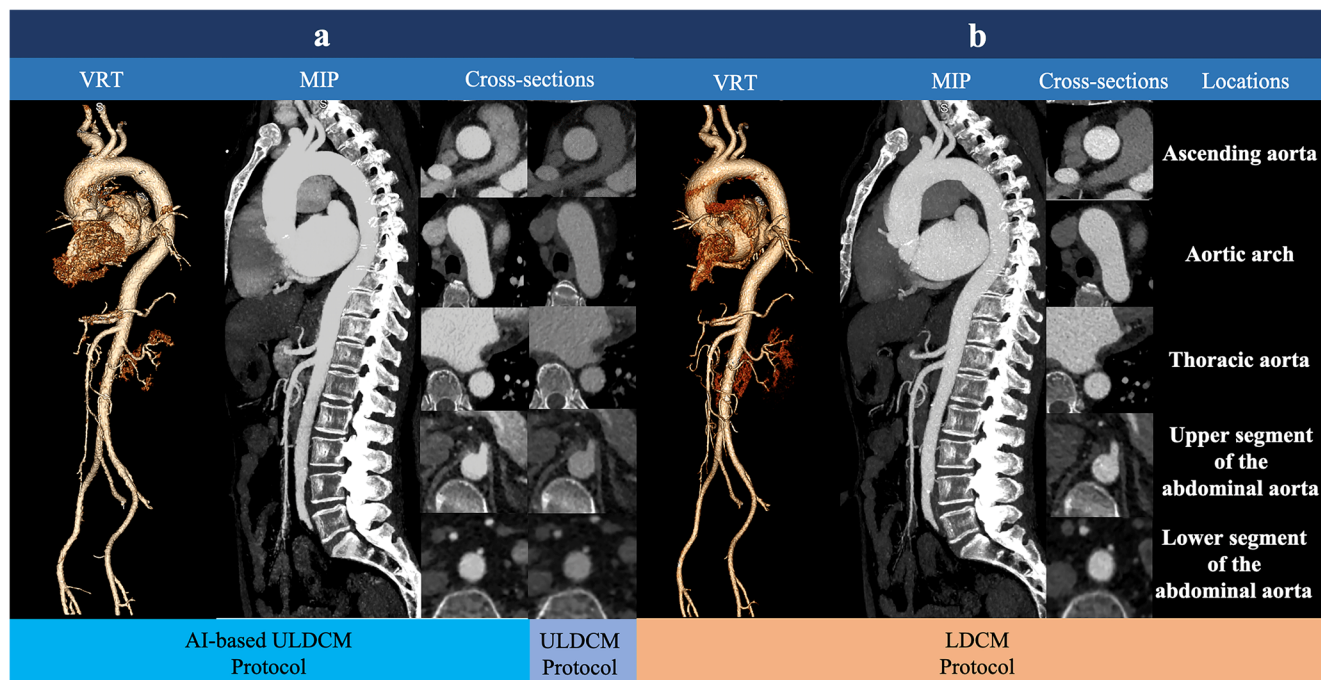


**Fig. 3** Examples of the image quality analysis in a patient with atherosclerosis. The volume rendering technique (VRT), maximum intensity projection (MIP), and orthogonal to the centerline orientated cross sections at the five locations of the artificial intelligence (AI)–based

based ultra-low-dose contrast medium (ULDCM) ACTA images and the ULDCM ACTA images (a). The VRT, MIP, and orthogonal to the centerline orientated cross sections at the five locations of the low-dose contrast medium (LDCM) ACTA images (b)

the aortic sinus), aortic arch, thoracic aorta (level of the 8th thoracic vertebra), the upper location of the abdominal aorta

(level of the celiac trunk opening), and the lower location of the abdominal aorta (2 cm above the iliac bifurcation); (2)

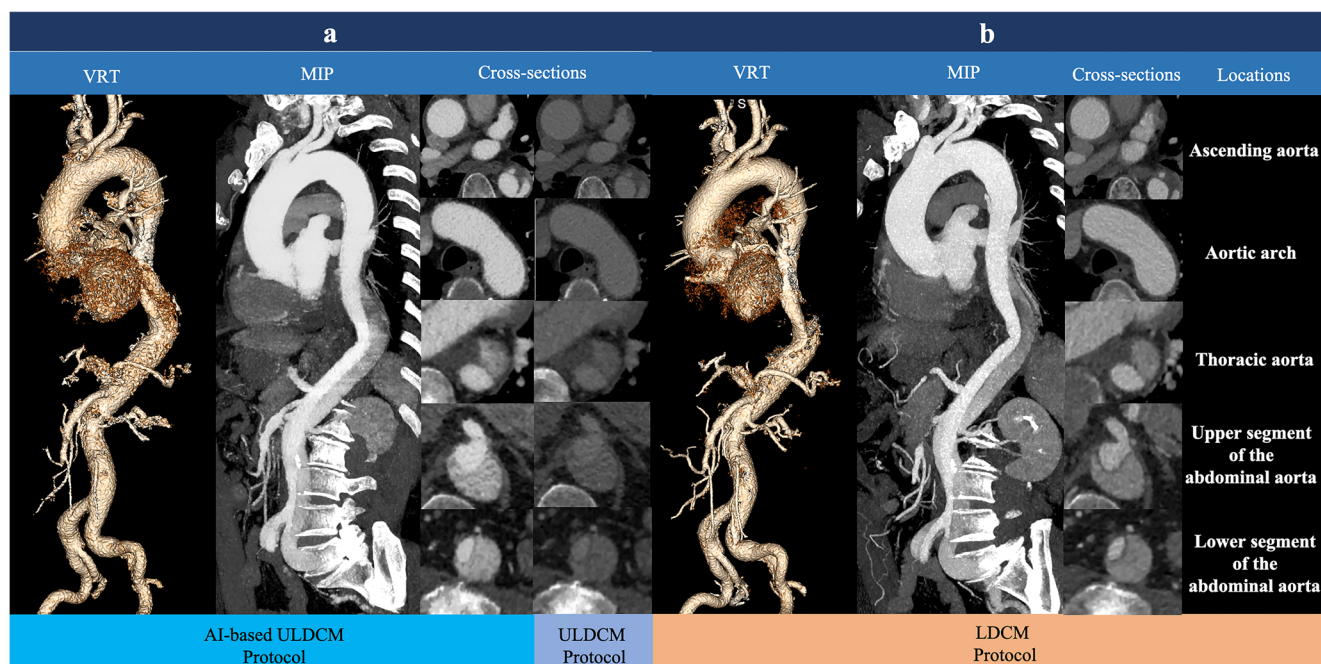


**Fig. 4** Examples of the image quality analysis in a patient with aortic dissection. The volume rendering technique (VRT), maximum intensity projection (MIP), and orthogonal to the centerline orientated cross sections at the five locations of the artificial intelligence (AI)–based

ultra-low-dose contrast medium (ULDCM) ACTA images and the ULDCM ACTA images (a). The VRT, MIP, and orthogonal to the centerline orientated cross sections at the five locations of the low-dose contrast medium (LDCM) ACTA images (b)

mean CT attenuation value ( $CT_{Mu}$ ) and SD value ( $SD_{Mu}$ ) of the skeletal muscle (trapezius muscle, deep back musculature, or erector spinae muscle) at the same level of the above aorta locations. The signal-to-noise ratio (SNR) and CNR were calculated using:

$$\text{SNR} = \frac{CT_{Ao}}{SD_{Mu}}$$

$$\text{CNR} = \frac{(CT_{Ao} - CT_{Mu})}{(SD_{Ao} + SD_{Mu})/2}$$

## Diagnostic accuracy analysis

Multiple aortic diseases were evaluated on the per-patient level using the anonymous AI-reconstructed ULDCM ACTA images, and consensus agreement should be reached. The anonymous LDCM ACTA images were also visually and separately evaluated for diagnosing the aortic diseases by the same two radiologists, who were blinded to the AI-based ULDCM ACTA results. To assess the diagnostic value, the AI-based ULDCM images and ULDCM images were compared with the LDCM images for detecting aortic diseases.

## Statistical analysis of the data

Statistical analyses were performed using SPSS (versions 25). The continuous data were expressed as mean  $\pm$  SD. The non-parametric subjective evaluation data were expressed as median with frequency. Differences in the mean values were analyzed using a paired *t* test in normally distributed data and Wilcoxon test in non-normally distributed data. The interobserver agreement of the objective image quality parameters was evaluated using the intraclass correlation coefficient (ICC). Three levels of ICC were defined as follows: moderate agreement ( $< 0.6$ ), good agreement (between 0.6 and 0.8), and very good agreement ( $> 0.8$ ). The diagnostic accuracy of the AI-based ULDCM images and LDCM images was compared

using the McNemar chi-square test. Cohen's kappa ( $k$ ) test was also used to evaluate the diagnostic ability of the AI-based ULDCM images and the ULDCM images, with kappa values  $\leq 0$  indicating no agreement, and  $0.0 < k \leq 0.2$  as poor,  $0.2 < k \leq 0.4$  as fair,  $0.4 < k \leq 0.6$  as moderate,  $0.6 < k \leq 0.8$  as substantial, and  $0.8 < k \leq 1.0$  as excellent agreement. A *p* value  $< 0.05$  was considered to be statistically significant.

## Results

### Patient baseline characteristics

ACTA was successfully performed in all enrolled patients. The patient demographics are presented in Table 1. No significant differences were seen between the ULDCM group and LDCM group in terms of radiation dose (all *p*  $> 0.05$ ), but the CM dose in the ULDCM group was much lower than that in the LDCM group (all *p*  $< 0.05$ ) (Table 2). The total radiation and CM dose each patient received are similar to those of the previous low-dose ACTA studies [27, 28].

### Qualitative image analysis

An overview of the qualitative CTA image analysis is given in Table 3. The subjective image quality score of each aortic location in the AI-based ULDCM group was higher than that in the ULDCM group (all *p*  $< 0.05$ ) but a little lower than that in the LDCM group (all *p*  $< 0.05$ ), owing to the slightly blurred blood vessel margins in AI-based ULDCM images. But all AI-based ULDCM and LDCM images met the diagnostic requirements (qualitative image quality score at each location in two groups  $\geq 3.0$ ). And we also did the subgroup analysis of qualitative image analysis in obese patients (BMI  $> 25$ ), whose results are similar to the findings described above (Table 4).

**Table 1** Patient demographic and pathologic information

	Training dataset (n = 100)	Validation dataset (n = 50)	<i>p</i> value
Age (years)	56.1 $\pm$ 14.9	60.3 $\pm$ 11.5	0.056
Sex (male:female)	75:25	36:14	—
Height (cm)	171.3 $\pm$ 7.9	169.0 $\pm$ 6.9	0.087
Weight (kg)	71.3 $\pm$ 10.6	68.9 $\pm$ 10.2	0.194
BMI (kg/m <sup>2</sup> )	24.3 $\pm$ 3.2	24.1 $\pm$ 2.9	0.701
Heart rate	72.2 $\pm$ 13.1	68.2 $\pm$ 12.5	0.075
Hypertension, n (%)	80 (80)	30 (60)	—
Diabetes, n (%)	6 (6)	6 (12)	—
Hyperlipidemia, n (%)	23 (23)	22 (44)	—
Smoking history, n (%)	22 (22)	26 (52)	—
Alcohol consumption, n (%)	8 (8)	28 (56)	—

**Table 2** Results of radiation dose and CM dose in the ULDCM group and LDCM group

	Training dataset ( <i>n</i> = 100)			Validation dataset ( <i>n</i> = 50)		
	ULDCM group	LDCM group	<i>p</i> value	ULDCM group	LDCM group	<i>p</i> value
<b>Radiation dose</b>						
CTDI <sub>vol</sub> (mGy)	3.8 ± 0.5	3.8 ± 0.5	0.798	2.9 ± 0.8	3.0 ± 0.8	0.083
DLP (mGy*cm)	276.2 ± 38.3	277.3 ± 37.2	0.065	209.6 ± 64.6	208.9 ± 66.7	0.570
SSDE (mGy)	5.1 ± 0.7	5.1 ± 0.7	0.849	4.0 ± 1.1	4.0 ± 1.1	0.094
ED (mSv)	4.1 ± 2.9	3.9 ± 0.5	0.348	2.9 ± 0.9	2.9 ± 0.9	0.466
<b>CM dose</b>						
Injection dose (ml, 320 mg I/ml)	14.6 ± 1.9	43.9 ± 5.7	< 0.001	14.5 ± 7.8	43.4 ± 5.2	< 0.001
Iodine intake (mg I/kg)	66.4 ± 8.3	199.2 ± 24.9	< 0.001	67.8 ± 7.4	203.5 ± 22.1	< 0.001

ULDCM ultra-low-dose contrast medium, LDCM low-dose contrast medium, CTDI<sub>vol</sub> CT dose index volume, DLP dose-length product, SSDE size-specific dose estimates, ED effective dose

## Quantitative image analysis

An overview of the quantitative image analysis is also provided in Table 3. The intra-vessel enhancement was adequate for all the analyzed arterial locations in both the AI-based ULDCM and LDCM images. Except for the image noise ( $p > 0.05$ ), each location of the AI-based ULDCM aortic images had a higher attenuation value and better enhancement appearance of the blood vessels than the ULDCM ACTA images and LDCM ACTA images (all  $p < 0.05$ ). The AI-based ULDCM images also had higher SNR and CNR values than the ULDCM images and LDCM images (all  $p < 0.05$ ). In the analysis of obese patients (BMI > 25), we also found the attenuation value, SNR, and CNR of the AI-based ULDCM aortic images are higher than those of the ULDCM images and LDCM images (all  $p < 0.05$ ) (Table 4). There were good interobserver agreements for the quantitative image analysis between the two readers (all ICC values  $> 0.7$ ,  $p < 0.001$ , Supplementary Table S1).

## Diagnostic accuracy of ACTA for aortic diseases

When compared with the LDCM images, the AI-based ULDCM images demonstrated good sensitivity, specificity, positive predictive value, and negative predictive value in the patient-based analysis. Owing to the poor image quality, the diagnostic ability of the ULDCM images was worse than that of the AI-based ULDCM images, especially the sensitivity (Table 5). An excellent agreement was perceived in detecting atherosclerosis, aortic aneurysms, aortic dissection, intramural hematoma, penetrating atherosclerotic ulcer, pseudoaneurysm, systemic diseases, and congenital abnormalities between the AI-based ULDCM group and the LDCM group (all  $K$ -values  $> 0.80$ ), but a fair agreement between the ULDCM group and the LDCM group (except for atherosclerosis and aortic dissection, all  $K$ -values  $\leq 0.40$ ). Furthermore, no

significant differences were seen between the AI-based ULDCM group and the LDCM group in any of the analyzed aortic disease diagnoses (all  $p > 0.05$ ).

## Discussion

To our knowledge, this preliminary study is the first clinical study of an AI-based visual enhancement algorithm on ULDCM ACTA images. Our Au-CycleGAN algorithm enabled improving the visual enhancement degree of ULDCM images and substantial reduction in CM dose to one-third of the CM dose used in the LDCM protocol without compromising the image quality or diagnostic accuracy.

The administration of CM during CTA can exacerbate the radiation-induced DNA damage as assessed by Piechowiak et al with  $\gamma$ H2AX foci formation. Therefore, the reduction of the CM dose not only contributes to the kidney function protection but also adds to the protection from radiation exposure [29].

The application of low voltage and IR techniques has significantly lowered the CM dose [3]. However, the image noise increases with the decrease in tube voltage, which may affect image post-processing and diagnosis. The low tube voltage is also considered unsuitable for patients with high BMI, and the ability of this method in reducing the iodine load is limited. Although the IR algorithm can effectively denoise in low-tube-voltage images, its denoising ability is also limited owing to its need to balance image noise, spatial resolution, and image texture. Using IR algorithms with higher weights can reduce the spatial resolution and create a visual plastic appearance, which may influence the image interpretation [16, 30].

Energy spectrum CT has also been exploited to reduce the CM dose [4], which has been demonstrated in abdominal and thoracic CTA [31, 32], including coronary CTA [33]. It provides better image quality compared to conventional

**Table 3** Results of qualitative and quantitative image analysis

Location	Parameters	AI-based ULDCM group (n = 50)	ULDCM group (n = 50)	LDCM group (n = 50)
Ascending aorta	Image quality score	3.9 ± 0.5	2.0 ± 0.5 <sup>#</sup>	4.4 ± 0.6*
	Attenuation (HU)	447.3 ± 39.6	151.8 ± 36.5 <sup>#</sup>	373.5 ± 69.2*
	Image noise (HU)	21.1 ± 4.4	19.7 ± 4.1 <sup>#</sup>	20.2 ± 3.2
	SNR	22.2 ± 5.6	8.2 ± 3.2 <sup>#</sup>	19.0 ± 5.0*
	CNR	19.0 ± 6.5	5.3 ± 2.2 <sup>#</sup>	13.5 ± 3.0*
Aortic arch	Image quality score	4.1 ± 0.4	2.1 ± 0.5 <sup>#</sup>	4.7 ± 0.5*
	Attenuation (HU)	464.5 ± 36.1	155.4 ± 39.8 <sup>#</sup>	373.8 ± 65.9*
	Image noise (HU)	20.8 ± 3.7	20.1 ± 3.0	20.4 ± 3.2
	SNR	23.1 ± 4.8	8.1 ± 2.8 <sup>#</sup>	18.9 ± 4.8*
	CNR	20.8 ± 6.2	5.1 ± 2.3 <sup>#</sup>	13.2 ± 3.1*
Thoracic aorta	Image quality score	3.9 ± 0.5	2.1 ± 0.5 <sup>#</sup>	4.4 ± 0.5*
	Attenuation (HU)	438.8 ± 52.6	155.6 ± 39.0 <sup>#</sup>	369.7 ± 65.3*
	Image noise (HU)	21.2 ± 4.2	20.2 ± 4.0	20.7 ± 3.5
	SNR	21.6 ± 5.2	8.2 ± 3.1 <sup>#</sup>	18.5 ± 5.2*
	CNR	16.5 ± 4.9	5.1 ± 2.2 <sup>#</sup>	12.3 ± 2.9*
The upper segment of the abdominal aorta	Image quality score	3.8 ± 0.5	1.8 ± 0.6 <sup>#</sup>	4.5 ± 0.5*
	Attenuation (HU)	427.9 ± 43.2	156.7 ± 40.7 <sup>#</sup>	367.8 ± 68.0*
	Image noise (HU)	23.4 ± 3.9	22.5 ± 3.2	23.2 ± 3.5
	SNR	18.8 ± 3.7	7.2 ± 2.4 <sup>#</sup>	16.4 ± 4.8*
	CNR	15.1 ± 4.0	4.5 ± 1.8 <sup>#</sup>	10.8 ± 2.4*
The lower segment of the abdominal aorta	Image quality score	3.8 ± 0.5	2.0 ± 0.5 <sup>#</sup>	4.3 ± 0.6*
	Attenuation (HU)	395.9 ± 46.5	166.1 ± 76.5 <sup>#</sup>	358.7 ± 73.9*
	Image noise (HU)	23.3 ± 4.7	22.4 ± 4.2	22.2 ± 3.7
	SNR	17.7 ± 4.4	7.7 ± 3.8 <sup>#</sup>	16.7 ± 5.0
	CNR	14.4 ± 3.8	5.3 ± 3.3 <sup>#</sup>	11.9 ± 3.3*

AI artificial intelligence, ULDCM ultra-low-dose contrast medium, LDCM low-dose contrast medium, SNR signal-to-noise ratio, CNR contrast-to-noise ratio

\* AI-based ULDCM group vs. ULDCM group,  $p < 0.05$ ; #AI-based ULDCM group vs. LDCM group,  $p < 0.05$

techniques while facilitating to reduce the CM dose. Nevertheless, energy spectrum CT technology is not widely used owing to its high cost. Moreover, monoenergetic reconstruction is time-consuming and is influenced by many factors, such as vendor, patient, and situation-specific factors [6]. Cross-scattered radiation is another challenge, which can produce artifacts and decrease the CNR of the images and affect the diagnostic accuracy [7]. Energy spectrum CT technology holds great promise for image reconstruction and CM dose reduction, but we also need greater effort to solve the above-mentioned technical problems.

Deep learning image reconstruction (DLIR) algorithms do not involve a trade-off between image noise and spatial resolution and thus are accurate and computationally efficient. DLIR can significantly reduce noise and create high-quality reconstructed images from low-quality images, which has been demonstrated in phantom studies and some latest clinical studies [16, 17, 34, 35]. What's more, in addition to its

advantages in suppressing the noise of low-tube-voltage CT images, AI also has the potential to further reduce the dose of CM. However, only a few AI studies have been published to further reduce the CM dose needed for current LDCM CTA imaging. Haubold et al evaluated the feasibility of reducing the dose of iodined CM in CT through virtual contrast-enhanced images using generative adversarial networks (GAN) and their algorithm reduced by 50% of the required amount of CM for CT while maintaining image quality and diagnostic accuracy. But not conducting true double examinations with and without CM dose reduction is the most significant limitation of their study. Whether their GAN-based approach would work in real CM dose reduction regimes should be further explored [36].

Different to other studies, we have successfully improved the enhancement degree of the real ULDCM ACTA images based on a new Au-CycleGAN algorithm, and drastically reduced the iodine load of patients receiving ACTA scans. The

**Table 4** Subgroup analysis of qualitative and quantitative image parameters in obese patients (BMI > 25)

Location	Parameters	AI-based ULDCM group (n = 16)	ULDCM group (n = 16)	LDCM group (n = 16)
Ascending aorta	Image quality score	3.9 ± 0.4	1.9 ± 0.6 <sup>#</sup>	4.4 ± 0.7*
	Attenuation (HU)	449.7 ± 33.2	151.2 ± 50.5 <sup>#</sup>	369.3 ± 61.5*
	Image noise (HU)	22.6 ± 4.4	21.0 ± 4.7	20.9 ± 3.0
	SNR	20.7 ± 4.6	8.0 ± 4.4 <sup>#</sup>	18.1 ± 4.3*
Aortic arch	CNR	17.6 ± 4.8	4.9 ± 2.7 <sup>#</sup>	12.8 ± 2.5*
	Image quality score	4.0 ± 0.4	2.1 ± 0.6 <sup>#</sup>	4.6 ± 0.5*
	Attenuation (HU)	462.9 ± 25.2	152.8 ± 53.1 <sup>#</sup>	365.9 ± 57.2*
	Image noise (HU)	23.2 ± 3.2	21.5 ± 2.7	21.4 ± 2.8
Thoracic aorta	SNR	20.4 ± 3.5	7.4 ± 3.2 <sup>#</sup>	17.5 ± 4.3*
	CNR	18.4 ± 5.9	4.6 ± 2.8 <sup>#</sup>	12.0 ± 2.5*
	Image quality score	3.8 ± 0.4	2.1 ± 0.6 <sup>#</sup>	4.3 ± 0.5*
	Attenuation (HU)	442.6 ± 30.1	154.0 ± 49.6 <sup>#</sup>	360.3 ± 56.0*
The upper segment of the abdominal aorta	Image noise (HU)	23.0 ± 4.2	21.8 ± 4.0	21.9 ± 3.8
	SNR	19.9 ± 4.0	7.5 ± 3.5 <sup>#</sup>	17.1 ± 4.7*
	CNR	15.4 ± 4.3	4.6 ± 2.5 <sup>#</sup>	11.6 ± 2.3*
	Image quality score	3.9 ± 0.3	1.8 ± 0.7 <sup>#</sup>	4.4 ± 0.5*
The lower segment of the abdominal aorta	Attenuation (HU)	435.3 ± 35.7	155.5 ± 55.0 <sup>#</sup>	360.1 ± 58.8*
	Image noise (HU)	24.6 ± 2.6	23.8 ± 2.8	25.8 ± 2.3
	SNR	17.9 ± 2.7	6.8 ± 3.0 <sup>#</sup>	14.1 ± 3.0*
	CNR	14.6 ± 3.7	4.2 ± 2.3 <sup>#</sup>	10.1 ± 2.0*

AI artificial intelligence, ULDCM ultra-low-dose contrast medium, LDCM low-dose contrast medium, SNR signal-to-noise ratio, CNR contrast-to-noise ratio

\* AI-based ULDCM group vs. ULDCM group,  $p < 0.05$ ; #AI-based ULDCM group vs. LDCM group,  $p < 0.05$

AI-based ULDCM images provided not only good image quality, but also diagnostic accuracy. Although the qualitative image quality score of the AI-based ULDCM group was a little lower than that of the LDCM group, owing to its slightly heterogeneous enhancement appearance and partially blurred blood vessel margins in some locations of the aorta, all the AI-based ULDCM images met the clinical diagnosis requirements. In order to minimize the radiation and CM dose in patients enrolled in our study, we made some concessions in subjective image quality. The qualitative image quality score could be further improved if we increased the CM dose appropriately in the current ULDCM protocol.

It is worth noting that the enhancement degree of the AI-based ULDCM images was higher than that of the LDCM images. This benefits from one of the strengths of our AI algorithm that it can adjust the attenuation value (HU) range of the ACTA images rationally, resulting in a higher attenuation value and better enhancement appearance of blood

vessels. However, no significant difference was seen in the image noise between the AI-based ULDCM group and the LDCM group since we did not acquire the raw data of these ACTA images and further denoising was not applied. Therefore, incorporating a noise and artifact reduction filter in our visual enhancement algorithm may be helpful to further increase the objective image quality.

The AI visual enhancement algorithm we designed is beneficial in patients with reduced or marginal renal function, and thyroid hyperfunction, and improves the safety of the ACTA scans. Our algorithm is also not dependent on patient weight and solves the problem of high CM dose needed for ACTA examination in patients with high BMI. Furthermore, our algorithm could be exploited in the ULDCM CTA examinations of other blood vessels too, such as the coronary artery, the pulmonary artery, the carotid artery, and others, and thus enabling more patients to benefit from this image reconstruction

**Table 5** The diagnostic parameters of AI-based ULDCM images and ULDCM images in the patient-based analysis

Diagnosis	AI-based ULDCM group (n = 50)			ULDCM group (n = 50)			AI-based ULDCM group (n = 50)			ULDCM group (n = 50)		
	Sensitivity	Specificity	Positive predictive value	Negative predictive value	Cohens' kappa (k) test	p value	Sensitivity	Specificity	Positive predictive value	Negative predictive value	Cohens' kappa (k) test	p value
Normal finding	4	7	3	1.00	0.98	0.75	1.00	0.847	< 0.001	0.67	0.89	0.29
Atherosclerosis	37	34	38	0.98	1.00	0.92	0.947	< 0.001	0.79	0.67	0.89	0.50
Aortic aneurysm	11	7	11	1.00	1.00	1.00	1.00	< 0.001	0.36	0.92	0.57	0.84
Aortic dissection	2	1	2	1.00	1.00	1.00	1.00	< 0.001	0.50	1.00	1.00	0.98
Intramural hematoma	4	2	4	1.00	1.00	1.00	1.00	< 0.001	0.25	0.98	0.50	0.94
Penetrating atherosclerotic ulcer	9	2	11	0.82	1.00	0.95	0.875	< 0.001	0.09	0.97	0.5	0.79
Pseudoaneurysm	4	1	4	1.00	1.00	1.00	1.00	< 0.001	0.25	1.00	1.00	0.94
Systemic diseases	1	0	1	1.00	1.00	1.00	1.00	< 0.001	0	1.00	—	—
Congenital abnormalities	1	0	1	1.00	1.00	1.00	1.00	< 0.001	0	1.00	—	—

AI artificial intelligence, ULDCM ultra-low-dose contrast medium, LDCM low-dose contrast medium

technology. Moreover, we will do further algorithm study based on energy spectrum CT to combine the benefits of AI and energy spectrum CT and to further reduce the CM dose needed for ACTA.

Our study still has some limitations. First, some distal branches of the aorta had a poor and heterogeneous enhancement appearance in the AI-based ULDCM images, which may affect the accuracy when assessing the lesions in these locations. Hence, we are planning to make improvements in further algorithm studies. Second, our algorithm might have improved the enhancement appearance (e.g., improved SNR and CNR), but we did not solve the fundamental problem of the noise since we did not acquire the raw data of the ACTA images. Third, we only assessed the diagnostic accuracy of the AI-based ULDCM images by comparing our findings with the LDCM results rather than using invasive aortic angiography as a reference standard. However, the accuracy and reproducibility of non-invasive ACTA have been demonstrated in many studies [37–40]. Besides, though the LDCM scan started one hour after the ULDCM scan, aiming to avoid the potential residual enhancement as much as possible, the repeated administration of CM may affect the assessment of quantitative image quality parameters. The influence of this potential drawback still needs to be revealed in a further study. Moreover, the number of cases was limited, which may not adequately represent all types of aortic diseases. And our algorithm is trained and tested on images generated from a single scanner from a single institution. Future multicenter studies with more cases (including aortic surgeries) are needed to further evaluate the feasibility of our AI algorithm in ACTA imaging with ULDCM.

In conclusion, the required dose of CM for full ACTA imaging can be reduced to one-third of the CM dose of conventional LDCM protocol while maintaining image quality and diagnostic accuracy using Au-CycleGAN algorithm. However, our algorithm still needs further improvement, and more data are required for its validation.

**Supplementary Information** The online version contains supplementary material available at <https://doi.org/10.1007/s00330-022-08975-1>.

**Acknowledgements** We are grateful to all the staff and epidemiologists who were involved in the care of our study subjects.

**Funding** This study has received funding from the National Natural Science Foundation of China (82271986, U1908211), the Capital's Funds for Health Improvement and Research Foundation of China (2020-1-1052), and the National Key Research and Development Program of China (2016YFC1300300).

## Declarations

**Guarantor** The scientific guarantor of this publication is Lei Xu.

**Conflict of interest** The authors of this manuscript declare no relationships with any companies whose products or services may be related to the subject matter of the article.

**Statistics and biometry** One of the authors (Nan Zhang) has significant statistical expertise.

**Informed consent** Written informed consent was obtained from all subjects (patients) in this study.

**Ethical approval** Institutional Review Board approval was obtained.

## Methodology

- prospective
- diagnostic or prognostic study
- performed at one institution

## References

1. Erbel R, Aboyans V, Boileau C et al (2014) 2014 ESC guidelines on the diagnosis and treatment of aortic diseases: document covering acute and chronic aortic diseases of the thoracic and abdominal aorta of the adult. The Task Force for the Diagnosis and Treatment of Aortic Diseases of the European Society of Cardiology (ESC). Eur Heart J 35:2873–2926
2. Knuuti J, Bengel F, Bax JJ et al (2014) Risks and benefits of cardiac imaging: an analysis of risks related to imaging for coronary artery disease. Eur Heart J 35:633–638
3. Masuda T, Funama Y, Nakaura T et al (2018) Radiation dose reduction with a low-tube voltage technique for pediatric chest computed tomographic angiography based on the contrast-to-noise ratio index. Can Assoc Radiol J 69:390–396
4. Lenga L, Albrecht MH, Othman AE et al (2017) Monoenergetic dual-energy computed tomographic imaging: cardiothoracic applications. J Thorac Imaging 32:151–158
5. Benz DC, Grani C, Hirt Moch B et al (2016) Minimized radiation and contrast agent exposure for coronary computed tomography angiography: first clinical experience on a latest generation 256-slice scanner. Acad Radiol 23:1008–1014
6. Albrecht MH, De Cecco CN, Schoepf UJ et al (2018) Dual-energy CT of the heart current and future status. Eur J Radiol 105:110–118
7. Schmidt B, Flohr T (2020) Principles and applications of dual source CT. Phys Med 79:36–46
8. Kahn CE Jr (2017) From images to actions: opportunities for artificial intelligence in radiology. Radiology 285:719–720
9. Anthimopoulos M, Christodoulidis S, Ebner L, Christe A, Mougiakakou S (2016) Lung pattern classification for interstitial lung diseases using a deep convolutional neural network. IEEE Trans Med Imaging 35:1207–1216
10. Baskaran L, Maliakal G, Al'Aref SJ et al (2020) Identification and quantification of cardiovascular structures from CCTA: an end-to-end, rapid, pixel-wise, deep-learning method. JACC Cardiovasc Imaging 13:1163–1171
11. Zhang N, Yang G, Zhang W et al (2021) Fully automatic framework for comprehensive coronary artery calcium scores analysis on non-contrast cardiac-gated CT scan: total and vessel-specific quantifications. Eur J Radiol 134:109420
12. van Velzen SGM, Lessmann N, Velthuis BK et al (2020) Deep learning for automatic calcium scoring in CT: validation using multiple cardiac CT and chest CT protocols. Radiology 295:66–79
13. Nakanishi R, Slomka PJ, Rios R et al (2021) Machine learning adds to clinical and CAC assessments in predicting 10-year CHD and CVD deaths. JACC Cardiovasc Imaging 14:615–625

14. Eisenberg E, McElhinney PA, Commandeur F et al (2020) Deep learning-based quantification of epicardial adipose tissue volume and attenuation predicts major adverse cardiovascular events in asymptomatic subjects. *Circ Cardiovasc Imaging* 13:e009829
15. Yang Q, Yan P, Zhang Y et al (2018) Low-dose CT image denoising using a generative adversarial network with Wasserstein distance and perceptual loss. *IEEE Trans Med Imaging* 37:1348–1357
16. Greffier J, Hamard A, Pereira F et al (2020) Image quality and dose reduction opportunity of deep learning image reconstruction algorithm for CT: a phantom study. *Eur Radiol* 30:3951–3959
17. Benz DC, Benetos G, Rampidis G et al (2020) Validation of deep-learning image reconstruction for coronary computed tomography angiography: impact on noise, image quality and diagnostic accuracy. *J Cardiovasc Comput Tomogr* 14:444–451
18. Brady SL, Kaufman RA (2012) Investigation of American Association of Physicists in Medicine Report 204 size-specific dose estimates for pediatric CT implementation. *Radiology* 265: 832–840
19. Shrimpton PC, Hillier MC, Lewis MA, Dunn M (2006) National survey of doses from CT in the UK: 2003. *Br J Radiol* 79:968–980
20. Liu T, Gao Y, Wang H et al (2020) Association between right ventricular strain and outcomes in patients with dilated cardiomyopathy. *Heart*. <https://doi.org/10.1136/heartjnl-2020-317949>
21. Nwabuo CC, Moreira HT, Vasconcellos HD et al (2019) Left ventricular global function index predicts incident heart failure and cardiovascular disease in young adults: the coronary artery risk development in young adults (CARDIA) study. *Eur Heart J Cardiovasc Imaging* 20:533–540
22. Karnik AA, Gopal DM, Ko D, Benjamin EJ, Helm RH (2019) Epidemiology of atrial fibrillation and heart failure: a growing and important problem. *Cardiol Clin* 37:119–129
23. Januzzi JL Jr, Prescott MF, Butler J et al (2019) Association of change in N-terminal pro-B-type natriuretic peptide following initiation of sacubitril-valsartan treatment with cardiac structure and function in patients with heart failure with reduced ejection fraction. *JAMA* 322:1085–1095
24. Desai AS, Solomon SD, Shah AM et al (2019) Effect of sacubitril-valsartan vs enalapril on aortic stiffness in patients with heart failure and reduced ejection fraction: a randomized clinical trial. *JAMA* 322:1077–1084
25. Stewart MH, Lavie CJ, Shah S et al (2018) Prognostic implications of left ventricular hypertrophy. *Prog Cardiovasc Dis* 61:446–455
26. Liu T, Song D, Dong J et al (2017) Current understanding of the pathophysiology of myocardial fibrosis and its quantitative assessment in heart failure. *Front Physiol* 8:238
27. Ippolito D, Talei Franzesi C, Fior D, Bonaffini PA, Minutolo O, Sironi S (2015) Low kV settings CT angiography (CTA) with low dose contrast medium volume protocol in the assessment of thoracic and abdominal aorta disease: a feasibility study. *Br J Radiol* 88: 20140140
28. Wei L, Li S, Gao Q, Liu Y, Ma X (2016) Use of low tube voltage and low contrast agent concentration yields good image quality for aortic CT angiography. *Clin Radiol* 71:1313 e1315–1313 e1310
29. Piechowiak EI, Peter JF, Kleb B, Klose KJ, Heverhagen JT (2015) Intravenous iodinated contrast agents amplify DNA radiation damage at CT. *Radiology* 275:692–697
30. Geyer LL, Schoepf UJ, Meinel FG et al (2015) State of the art: iterative CT reconstruction techniques. *Radiology* 276:339–357
31. Johansen CB, Martinsen ACT, Enden TR, Svanteson M (2022) The potential of iodinated contrast reduction in dual-energy CT thoracic angiography; an evaluation of image quality. *Radiography (Lond)* 28:2–7
32. Albrecht MH, Trommer J, Wichmann JL et al (2016) Comprehensive comparison of virtual monoenergetic and linearly blended reconstruction techniques in third-generation dual-source dual-energy computed tomography angiography of the thorax and abdomen. *Invest Radiol* 51:582–590
33. Yi Y, Zhao XM, Wu RZ et al (2019) Low dose and low contrast medium coronary CT angiography using dual-layer spectral detector CT. *Int Heart J* 60:608–617
34. Park C, Choo KS, Jung Y, Jeong HS, Hwang JY, Yun MS (2021) CT iterative vs deep learning reconstruction: comparison of noise and sharpness. *Eur Radiol* 31:3156–3164
35. Sun J, Li H, Gao J et al (2021) Performance evaluation of a deep learning image reconstruction (DLIR) algorithm in “double low” chest CTA in children: a feasibility study. *Radiol Med* 126:1181–1188
36. Haubold J, Hosch R, Umutlu L et al (2021) Contrast agent dose reduction in computed tomography with deep learning using a conditional generative adversarial network. *Eur Radiol* 31:6087–6095
37. Hagan PG, Nienaber CA, Isselbacher EM et al (2000) The International Registry of Acute Aortic Dissection (IRAD): new insights into an old disease. *JAMA* 283:897–903
38. Parker MS, Matheson TL, Rao AV et al (2001) Making the transition: the role of helical CT in the evaluation of potentially acute thoracic aortic injuries. *AJR Am J Roentgenol* 176:1267–1272
39. Quint LE, Francis IR, Williams DM et al (1996) Evaluation of thoracic aortic disease with the use of helical CT and multiplanar reconstructions: comparison with surgical findings. *Radiology* 201: 37–41
40. Einstein AJ, Weiner SD, Bernheim A et al (2010) Multiple testing, cumulative radiation dose, and clinical indications in patients undergoing myocardial perfusion imaging. *JAMA* 304:2137–2144

**Publisher's note** Springer Nature remains neutral with regard to jurisdictional claims in published maps and institutional affiliations.

Springer Nature or its licensor (e.g. a society or other partner) holds exclusive rights to this article under a publishing agreement with the author(s) or other rightsholder(s); author self-archiving of the accepted manuscript version of this article is solely governed by the terms of such publishing agreement and applicable law.